Journal of Engineering Sciences
Vol 10, Issue 12, DEC/2019
ISSN NO:0377-9254

ANALYSIS OF TRANSFORMERLESS UPFC BASED ON FUZZY CONTROLLER

[1]M. Santhosh Kumar, [2]Dr V. Usha Reddy
[1]PG Student, Dept of EEE, SVU College of Engineering, Tirupati, India
E-mail: mskumar20696@gmail.com
[2]Assistant Professor, Dept of EEE, SVU College of Engineering, Tirupati, India,
E-mail: vyza_ushareddy@yahoo.co.in

***Abstract*— The existing transformerless Unified Power Flow Controller (UPFC) controllers have some disadvantages, such as presence of steady state oscillations and slow system dynamic response. To overcome this problem, a transformerless UPFC with fuzzy logic controller has been proposed which can have the capability to control the parameters of the transmission line and mitigate the harmonics present in the transmission line. This paper mainly focuses on low total harmonic distortion and high efficiency. The transformerless UPFC with proposed control approach is demonstrated using MATLAB/ SIMULINK and both the steady state and dynamic response results are shown.**

Keywords— Unified power flow controller (UPFC), cascade multilevel inverter, fuzzy logic controller, total harmonic distortion.

1. INTRODUCTION

The unified power flow controller (UPFC) has the ability to control, concurrently or particularly, all the parameters affecting power flow in the transmission line (i.e., voltage, impedance, and phase shift) [1]-[2]. The traditional UPFC includes back-to-back connected inverters which shares a common dc-link, as given in Fig. 1. A series voltage injected from inverter-2 may be at any angle with reference to the line current that gives greater flexibility and controllability to control power flows in the transmission line. The resultant active power at the terminals of inverter-2 is supplied or absorbed by means of inverter-1 via the dc-link. Thus, UPFC is ample and flexible ac transmission system device. It can reduce congestions and improves the transmission capability. UPFC requires two high voltage and high power inverters.

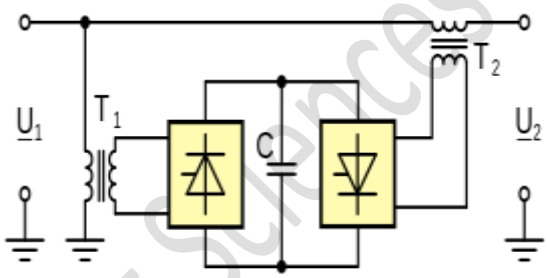

Fig. 1. Conventional UPFC.

The high-voltage and high power inverters must use robust and complex zigzag transformers to attain their required VA ratings and voltage waveforms. Zigzag transformers have some disadvantages such as high cost (30–40% of total cost), very lossy (50% of total power loss), cumbersome (40% of total area & 90% of total s/m weight) and high chances of getting fail [3]. Furthermore, the zigzag transformer based UPFC has too slow in dynamic response because of large time constant due to transformer saturation, magnetizing current, and surge voltage [4].

By investigating above problems the cascade multilevel inverter (CMI) is the simplest and realistic inverter technology to reach such high voltage levels without using transformers, a large number of semiconductor devices, or a big number of capacitors [5]. However, the CMIs couldn't be immediately used due to the fact the traditional UPFC requires inverters configured back-to-back to deal with real power flow.

To eliminate the above problem, a transformerless UPFC based on a configuration of two CMIs [6] has been proposed, which is shown in Fig. 2(a) and main system parameters for prototype is shown in Table I.

As shown in Fig. 2(a), the transformerless UPFC consists of two CMIs, one is series CMI, which is connected in series with the transmission line; whereas the other, shunt CMI is connected in parallel to the sending end after series CMI. Every CMI is composed of a series of cascaded H-bridge modules like shown in Fig. 2(b). The new UPFC has several advantages over the conventional UPFC such as good modular design, less weight, extremely good efficiency, high reliability, low cost, and a fast dynamic response.

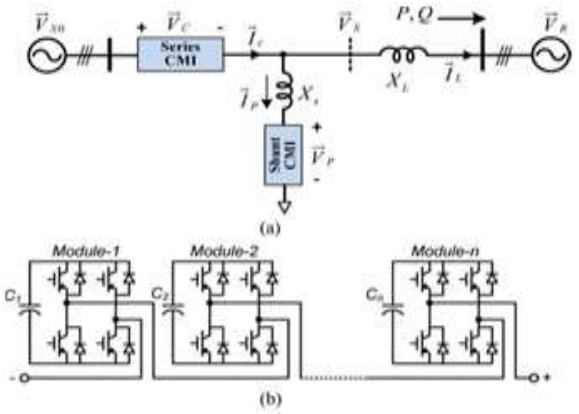

Fig. 2. Transformerless UFPC (a) System configuration (b) H-bridge modules

TABLE-I System Parameters for 13.8-kV Prototype

Parameter	Value
System power rating	2 MVA
V_{S0} rms	13.8 kV
Max series CMI current, I_C rms	84 A
Max shunt CMI current, I_P rms	42 A
V_{dc} (Shunt)	600 V
V_{dc} (Series)	600 V
H-bridge dc capacitance	2350 μF
No. of H-bridges per phase (Shunt)	20
No. of H-bridges per phase (Series)	10

The operational range and desired VA rating for series and shunt CMIs were studied in [7]. However, still there are some demanding situations for this transformerless UPFC such as modulation of the CMI for low THD of output voltage and improving dynamic response. So, this paper focuses on the modulation and control technique for the transformerless UPFC based on fuzzy controller to deal with abovementioned challenges. The functionality of the UPFC with proposed method is verified at voltage level 4160 V, and results of both the steady-state and dynamic responses will be presented in the later sections.

2. PRINCIPLE OF OPERATION OF TRANSFORMERLESS UPFC

The transformerless UPFC with this particular configuration of the series and shunt CMIs has some characteristics such as high efficiency, extremely high reliability, and rapid dynamic response.

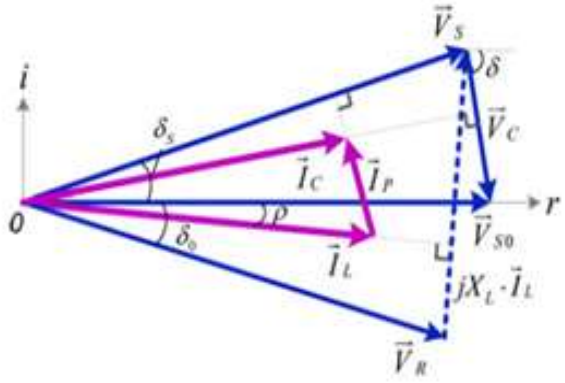

Fig. 3. Phasor diagram of transformerless UPFC

The phasor diagram of the UPFC is shown in Fig. 3, where $\vec{V}_{so}$ and $\vec{V}_R$ are the original sending-end and receiving-end voltages, respectively. $\vec{V}_{so}$ is associated with real axis, which means its phase angle is zero. By controlling the series CMI a desired voltage $\vec{V}_c$ is generated for obtaining the new sending-end voltage $\vec{V}_s$, which in turns, control both active and reactive power flows in the transmission line. On the other hand, a current $\vec{I}_P$ is injected by the shunt CMI to the new sending-end bus, which makes zero active power into both CMIs, which in turn makes the series CMI current $\vec{I}_c$ and the shunt CMI current $\vec{I}_P$ be perpendicular to their respective voltages $\vec{V}_c$ and $\vec{V}_s$. Thus, both the series and the shunt CMIs provide the reactive power only.

The transmitted real power P and reactive power Q in the line with the UPFC may be expressed from figs. 2 & 3, as

$$P + jQ = \vec{V}_R \cdot \left(\frac{\vec{V}_{so} - \vec{V}_C - \vec{V}_R}{jX_L}\right)^*$$

$$= \left(-\frac{V_{so}V_R}{X_L} sin\delta_0 + \frac{V_C V_R}{X_L} sin(\delta_0 - \delta)\right)$$

$$+ j\left(\frac{V_{so}V_R cos\delta_0 - {V_R}^2}{X_L} - \frac{V_C V_R}{X_L} cos(\delta_0 - \delta)\right) \quad (1)$$

Where symbol $*$ represents the conjugate of a complex number; δ_0 is the phase angle of the receiving-end voltage V_R; δ is the phase angle of the series CMI injected voltage V_C ; X_L is the equivalent transmission line impedance.

Real and reactive powers, P_0 and Q_0 with the uncompensated system ($V_C = 0$) are

$$\begin{cases} P_0 = -\frac{V_{so}V_R}{X_L} sin\delta_0 \\ Q_0 = \frac{V_{so}V_R cos\delta_0 - {V_R}^2}{X_L} \end{cases} \quad (2)$$

The net differences between the powers of system without the UPFC (2) and with the UPFC (1) are the controllable real and reactive powers, P_C and Q_C by the UPFC and can be expressed as

$$\begin{cases} P_C = -\frac{V_C V_R}{X_L} sin(\delta_0 - \delta) \\ Q_C = -\frac{V_C V_R}{X_L} cos(\delta_0 - \delta) \end{cases} \quad (3)$$

Therefore, we can rewrite (1) as

$$P + jQ = \underbrace{\left(\frac{-\frac{V_{so}V_R}{X_L} sin\delta_0}{P_0} + \frac{\frac{V_C V_R}{X_L} sin(\delta_0 - \delta)}{P_C}\right)}_{} +$$

$$j\left(\frac{\frac{V_{so}V_R cos\delta_0 - {V_R}^2}{X_L}}{Q_0} - \frac{\frac{V_C V_R}{X_L} cos(\delta_0 - \delta)}{Q_C}\right)$$

(4)

Both the amplitude V_C and phase angle δ of the UPFC injected voltage $\vec{V}_C$ can be any values as desired, the transformerless UPFC provides a controllable range of ($-V_C V_R/X_L$) to ($+V_C V_R/X_L$) for both real and reactive powers, P_C and Q_C, which are independent of voltage magnitude and phase angle of the original sending end voltage. By above summary (1)–(4) one can say that the functionality of the new UPFC has same as the traditional UPFC.

The series CMI voltage $\vec{V}_C$ is injected according to transmission line real/reactive power command, which can be calculated from (3).

$$\vec{V}_C = V_C \lfloor \delta = \frac{X_L}{V_R} \sqrt{{P^2}_C + {Q^2}_C} \left\lfloor \left(\delta_0 - \arctan\left(\frac{P_C}{Q_C}\right)\right)\right. \quad (5)$$

Once the series CMI injected voltage $\vec{V}_C$ is decided by (5), the new sending-end voltage and the transmission line current will be calculated accordingly.

$$\vec{V}_S = V_S \lfloor \delta_s = \vec{V}_{S0} - \vec{V}_C \quad (6)$$

Where

$$\begin{cases} V_S = \sqrt{(V_{SO} - V_C cos\delta)^2 + (V_C sin\delta)^2} \\ \delta_S = \arctan((-V_C sin\delta)/(V_{S0} - V_C cos\delta)) \end{cases} \quad (7)$$

And $\vec{I}_L = I_L \angle\rho$, where

$$\begin{cases} I_L = \left(\frac{\sqrt{(V_C sin\delta + V_R sin\delta_0)^2 + (V_{S0} - V_C cos\delta - V_R cos\delta_0)^2}}{X_L}\right) \\ \rho = \arctan\left(\frac{V_{S0} - V_C cos\delta - V_R cos\delta_0}{V_C sin\delta + V_R sin\delta_0}\right) \end{cases} \quad (8)$$

The current $\vec{I}_P$ injected by shunt CMI decouples the series CMI current $\vec{I}_C$ from the line current $\vec{I}_L$. Thus, zero real power exchange between both the series and the shunt CMIs can be achieved. Therefore, we have

$$\begin{cases} P_{se} = \vec{V}_C . \vec{I}_C = 0 \\ P_{sh} = \vec{V}_S . \vec{I}_P = 0 \end{cases} \quad (9)$$

Which means the series CMI current $\vec{I}_C$ and the shunt CMI current $\vec{I}_P$ should be perpendicular to

their voltages $\vec{V}_C$ and $\vec{V}_S$ respectively, as shown in Fig. 3. The shunt CMI output current can be calculated as

$$\vec{I}_P = I_P \angle \Theta_{Ip} \quad (10)$$

Where,

$$\begin{cases} I_P = I_L \left(\frac{\cos(\rho - \delta_S)}{\tan(\delta - \delta_S)} - \sin(\rho - \delta_S) \right) \\ \Theta_{Ip} = 90 + \delta_S \end{cases} \quad (11)$$

In precise, there are two important steps for the operation of the UPFC, which are calculation of injected voltage $\vec{V}_C$ for series CMI according to the real/reactive power demand over the transmission line(5) and calculation of injected current $\vec{I}_P$ for shunt CMI from (10) and (11) by making zero real power in both series and shunt CMIs [15].

3. FUNDAMENTAL FREQUENCY MODULATION (FFM) FOR CMIS

Mostly, the modulation for CMIs can be classified into two main categories. They are FFM and pulse width modulation (PWM). On comparing both, the FFM has much lower switching loss, making it more attractive for the UPFC and other high-voltage & high-power applications.

FFM will be designed with high number of H-bridge modules. Particularly, switching angles of all 10 series H-bridge modules and 20 shunt H-bridge modules will be optimized for achieving extremely low THD. Moreover, it will also shows that CMIs with FFM could achieve fast dynamic response (<8 ms) [8]-[9].

The principle of operation of FFM is shown in fig. 4. Where phase a_n output voltage of an 11-level CMI given as an example. A stair-case voltage waveform, V_a could be generated when each of five H-bridge modules generates a quasi-square wave, V_{H1}, V_{H2}, . . . , V_{H5}. Each H-bridge has the identical dc link voltage V_{dc} for the design scrutiny. Several approaches have been studied [10]-[11] to decide the switching angles of H-bridge modules for minimum THD.

The Fourier series expansion of the CMI output voltage shown in Fig. 4 is

$$V_a(\omega t) = \sum_{n=1}^{\infty} V_{an} . \sin(n\omega t) ,$$

$$V_{an} = \begin{cases} \frac{4}{n\pi} \sum_{k=1}^{s} V_{dc} \cos(n\alpha_k), \text{for odd } n \\ 0, \qquad \text{for even } n \end{cases} \quad (12)$$

Here n is harmonic number, *s* is number of H-bridge modules, and α_k represents the switching angle for the k_{th} H-bridge module.

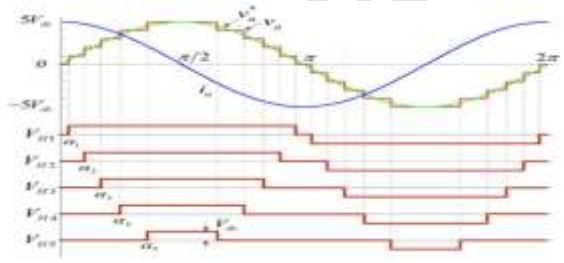

Fig. 4. Principle of operation of FFM

The THD of line voltage can be expressed as follows

$$THD = \frac{1}{V_{a1}} \sqrt{\sum_{n=5,7,11,..}^{\infty} V^2{}_{an}} \quad (13)$$

The value of THD is decreased with increasing number of H-bridge modules (*s*). When $s \geq 15$, the THD will be smaller than 1% [12].

4. CONTROL OF PROPOSED UPFC

A. Dynamic Models of UPFC System

All the equations derived from the phasor diagram in Section 2 are limited to steady-state analysis. To devise the vector-oriented control for the transformerless UPFC by considering both steady-state and dynamic performance, the dynamic modules are essential [15]. These models are based on synchronous (dq) frame of reference. Phase shift of the original sending-end voltage $\vec{V}_{so}$ is obtained

from a digital PLL, which can be used for abc to dq transformation. The dynamic model from the new sending-end bus to receiving-end bus is given as

$$\begin{cases} V_{sd} = R_L i_{Ld} + L_L \frac{di_{Ld}}{dt} - \omega L_L i_{Lq} + V_{Rd} \\ V_{sq} = R_L i_{Lq} + \frac{L_L di_{Lq}}{dt} + \omega L_L i_{Ld} + V_{Rq} \end{cases} \quad (14)$$

The new sending-end voltage $\vec{V}_S$ is equal to original sending-end voltage $\vec{V}_{SO}$ minus injected voltage $\vec{V}_C$ by series CMI, so we have

$$\begin{cases} V_{Cd} = V_{s0d} - V_{Sd} \\ V_{Cq} = V_{s0q} - V_{Sq} \end{cases} \quad (15)$$

The model from the new sending-end to shunt CMI is

$$\begin{cases} V_{sd} = R_s i_{Pd} + L_s \frac{di_{Pd}}{dt} - \omega L_s i_{Pq} + V_{Pd} \\ V_{sq} = R_s i_{Pq} + L_s \frac{di_{Pq}}{dt} + \omega L_s i_{Pd} + V_{pq} \end{cases} \quad (16)$$

B. Power Flow Control

It is necessary to implement a control system that can independently control both the real power P and reactive power Q over the line. Fig. 5 shows the overall control system, which is divided into three stages. They are:

Stage I: *The calculation from P*/Q* to* $\overrightarrow{V^*_{C0}}$ *and* $\overrightarrow{I^*_{p0}}$. As said above, $\overrightarrow{V^*_{C0}}$ is the injected voltage of series CMI that can be generated according to the power flow demand, while $\overrightarrow{I^*_{p0}}$ is injected current of shunt CMI, used to maintain zero real power for both CMIs. Calculating $\overrightarrow{V^*_{C0}}$ is shown in Fig. 6(a). Line current reference I^*_{Ld}/I^*_{Lq} is calculated from the P^*/Q^* reference and then the d-axis and q-axis components of series voltage V^*_{cod}, V^*_{C0q} are calculated from (15) & (16). The line current is controlled in a way to decouple feed forward control, achieving better dynamic response.

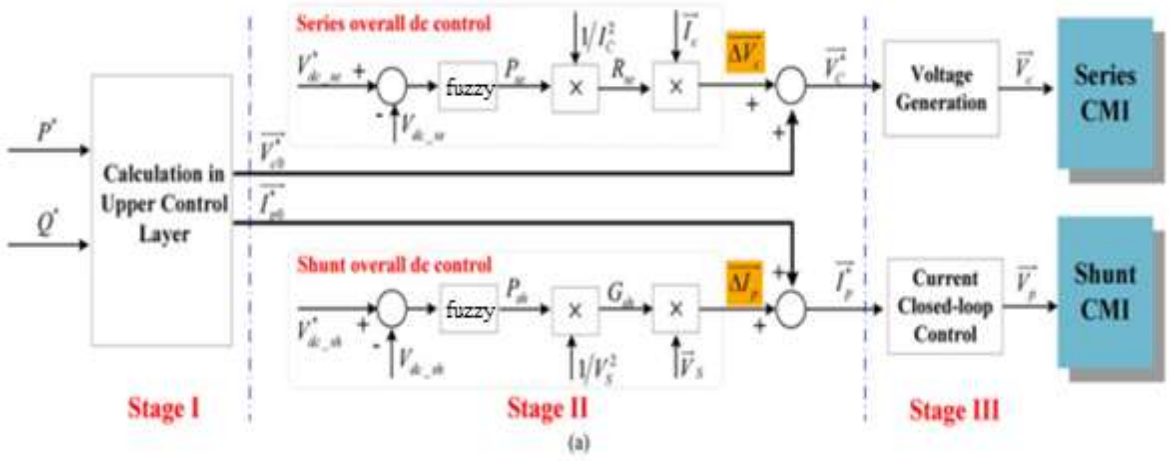

Fig. 5. Control diagram for power flow

Journal of Engineering Sciences
Vol 10, Issue 12, DEC/2019
ISSN NO:0377-9254

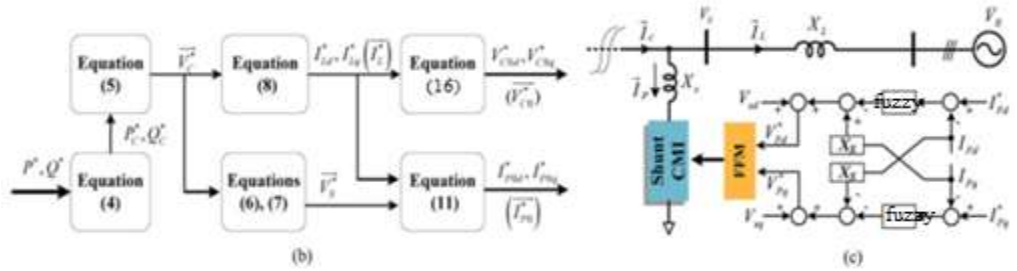

Fig. 6. (a) Calculation from P */Q* to $\overrightarrow{V^*_{C0}}$ and $\overrightarrow{I^*_{p0}}$, (b) Closed-loop control for shunt CMI.

Stage II: *Dc-link voltage regulation*. As mentioned earlier, the dc-link voltage cannot be maintained due to the reason that the CMIs always have a power loss. To control dc-link voltage with better results, two variables $\overrightarrow{\Delta V_C}$ and $\overrightarrow{\Delta I_P}$ were introduced as shown in Fig. 5 (a). Where, $V^*_{dc\text{-}sh}$ and $V^*_{dc\text{-}se}$ are dc voltage references for shunt and series CMIs, correspondingly; $V_{dc\text{-}sh}$ and $V_{dc\text{-}se}$ are the averaged dc feedback voltages of shunt and series CMIs, respectively. Considering the series CMI, P_{se} is the output of overall dc-link voltage regulation loop, R_{se} is calculated by dividing P_{se} by I^2_C and finally $\overrightarrow{\Delta V_C}$ is the product of R_{se} and $\overrightarrow{I_C}$. The introduced $\overrightarrow{\Delta V_C}$ is always in phase with series CMI $\overrightarrow{I_C}$. The dc-link can be balanced when P_{se} is equal to P_{loss}. In a similar way $\overrightarrow{\Delta I_P}$ is introduced by the shunt CMI, for dc-link voltage control. The current control loop has been designed for good dynamic response (<8 ms).

Stage III: *Generation of voltage and current for series and shunt CMIs*. The output voltage of series CMI could be directly generated from the reference $\overrightarrow{V^*_C}$ by FFM. Decoupling feedback current control is used to control the output current of shunt CMI by the reference current $\overrightarrow{I^*_P}$, as shown in Fig. 6(c) [13].

5. DESIGN OF FLC USING MATLAB

The FLC (Fuzzy Logic Controller) based transformerless UPFC is developed by using MATLAB/SIMULINK. The FLC has low settling time and steady state errors when it compared with other controllers. In general, fuzzification, rule-base/inference system and defuzzification steps are the three steps of the modeling of FLC [16]. Fuzzification process is a continuous transition of inputs from natural domain to the fuzzy domain through a set of membership functions.

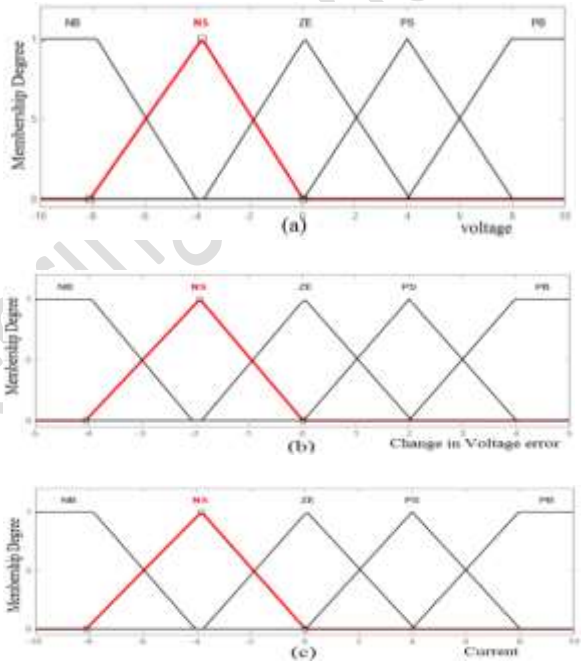

Fig. 7. Membership functions (a) Error, (b) Change in Error and (c) Output

Triangular membership functions are used for the input and output parameters as it gives fast response, simple calculation, simple coding and easy implantation. The input variables such as error and error rate are expressed in terms of fuzzy set with the linguistic terms NB, NS, ZE, PS, and PB in Mamdani fuzzy inference system. The number of linguistic variables for input and output is assumed as 5.Thus, the numbers of rules formed are 25. Also, all rules has similar weights (WI = 1) to keep consistency between rules and are summarized in Table II.

TABLE-II

Fuzzy Controller Rules

E / CE	NB	NS	ZE	PS	PB
NB	NB	NB	NB	NS	ZE
NS	NB	NB	NS	ZE	PS
ZE	NB	NS	ZE	PS	PB
PS	NS	ZE	PB	PB	PB
PB	ZE	PS	PB	PB	PB

The fuzzy rules are implemented based on IF-THEN rules. The fuzzy rules are used to assign outputs for the input signals. For instance, in controller a rule is written as follows:

IF error is NB and error-rate is PB, THEN output is ZE

Finally, defuzzification process is continued in order to convert the fuzzy linguistic variables to real crisp values. This research uses Centroid as a defuzzification method. The inputs are related with the logical AND/OR operators. AND logic gives the output as minimum value of the input and OR logic produces the output as maximum value of input.

6. SIMULATION RESULTS

In order to check the functionality of the UPFC with proposed modulation and control algorithm, a 4160-V test setup has been devised and shown in Fig. 8(a), and the system parameters are given in Table III. Fig. 8(b) shows the corresponding equivalent circuit, which is equivalent to the circuit design shown in Fig. 2(a). From fig. 8(b), we can say the receiving-end voltage $\overrightarrow{V_R}$ has same amplitude as original sending-end voltage $\overrightarrow{V_{SO}}$, but 30° phase lagging, which is introduced by transformer 2 with Y/Δ configuration.

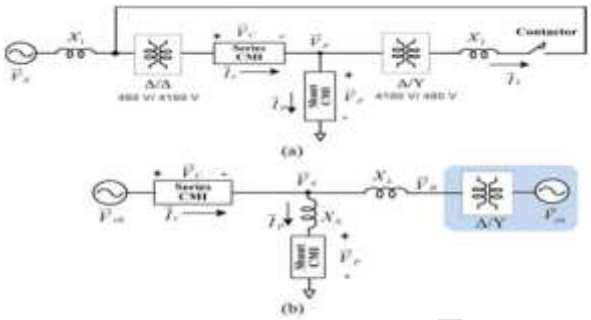

Fig. 8. Test setup. (a) Circuit configuration and (b) corresponding equivalent circuit

The basic functions of the UPFC have been tested based on above test setup and some simulation results are also given in this section.

TABLE III

System parameters for test setup

Parameter	Value
Grid Voltage (V_g)	480 V
Rated Frequency	60 Hz
V_{dc} of each shunt and series H-bridge	600 V
No. of H-bridges per phase for Shunt and Series	6 & 3
Transformer 1 (Δ/Δ) & Transformer 2 (Y/Δ)	480 V/ 4160 V, 75 kVA
Dc capacitance of each H-bridge	2350 μF
Rated line current	10 A
Reactor X_1	2.5 mH
Reactor X_2	3.2 mH
Leakage inductance of Transformer 1 (Δ/Δ) & Transformer 2 (Y/Δ)	35 mH (6% pu)
Equivalent line inductance X_L	0.31 H (50% pu)
Equivalent shunt filter inductance X_S	0.22 H (36% pu)

A. Phase Shifting

The UPFC can acts as a phase angle regulator that achieves the desired phase shift either leading or lagging of the original sending-end voltage with no change in magnitude. Three operating points with different phase shifts are considered and shown in Fig. 9.

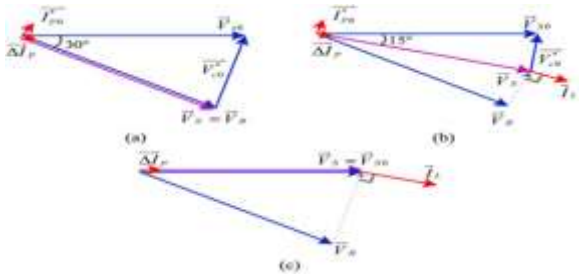

Fig. 9. Operating points with different phase shifting cases: (a) case A1: 30°, (b) case A2: 15 ° and (c) case A3: 0°.

Some discussions about the test results are given as follows:

i. The experimental waveforms from case A1 to case A2 is shown in Fig. 10. As mentioned earlier, there is already a 30° phase difference between the original sending-end voltage $\overrightarrow{V_{SO}}$ and the receiving-end voltage $\overrightarrow{V_R}$. In case A1, series CMI injected a voltage $\overrightarrow{V_C}$ to shift $\overrightarrow{V_{So}}$ by 30° lagging, which makes $\overrightarrow{V_{So}}$ = $\overrightarrow{V_R}$. Therefore, the resulting line current in this case is almost zero. In case A2, new sending-end voltage $\overrightarrow{V_S}$ is shifted from $\overrightarrow{V_{So}}$ by 15°, hence, there exists a 15° phase difference between $\overrightarrow{V_{So}}$ and $\overrightarrow{V_R}$. This will result in about 7-A line current. Fig. 10(a) and 10(b) shows the simulation results and it also shows that the current smoothly and quickly raised from zero to 7A, when the operating point is changed from case A1 to A2.

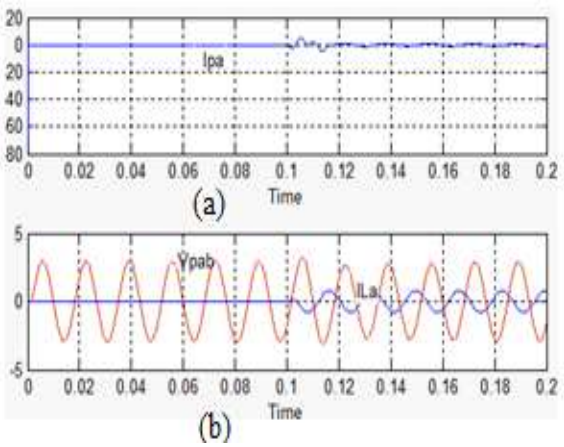

Fig. 10. Waveforms of UPFC operating from case A1 to case A2: (a) Shunt CMI phase current I_{Pa} (b) shunt CMI line voltage $V_{P\,ab}$, shunt CMI line current $I_{La.}$

ii. In the same way, the results of UPFC operating from case A2 to case A3 are shown in Fig. 11.

Waveforms V_{pa} and V_{pb} are generated by the FFM with optimized switching angles. In case A3, phase shifting is zero degree, which indicates a system without compensation. So, $\overrightarrow{V_S}$ = $\overrightarrow{V_{So}}$, and the phase angle between $\overrightarrow{V_{So}}$ and $\overrightarrow{V_R}$ is 30°. As a result the amplitude of current is changed to 14 A.

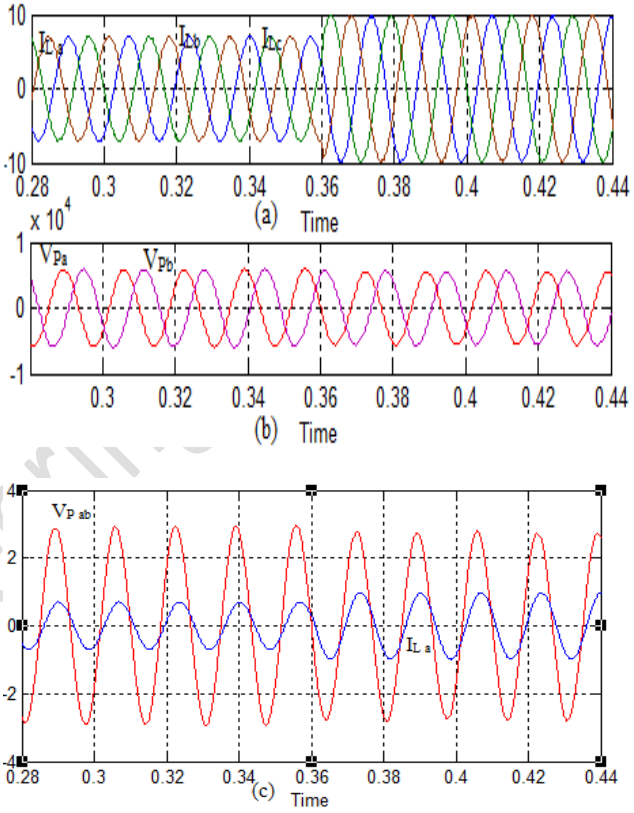

Fig. 11. Waveforms of UPFC operating from case A2 to case A3: (a) Shunt CMI line current I_{La}, I_{Lb}, I_{Lc} (b) Shunt CMI phase voltage V_{Pa}, V_{Pb} (c) Line current I_{La} and shunt CMI line voltage V_{Pab}.

iii. The measured dynamic response when operating point changing from case A2 to case A3 is shown in fig. 12. Here the amplitude of current would change from 7 to 14 A. The UPFC has achieved fast dynamic response, with response time <8 ms.

iv. Simulation results of dc capacitor voltage of both series and shunt CMIs when operating point changing from case A2 to case A3 is shown in fig. 13. During the transition, the dc link voltage almost kept constant, which means the dc link voltage is independent of operating points.

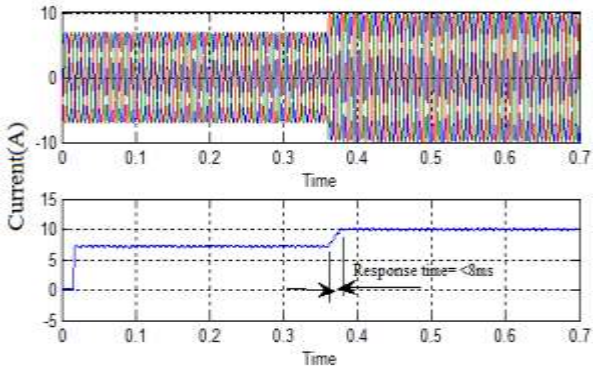

Fig. 12. Dynamic response when operating point changes from case A2 to case A3.

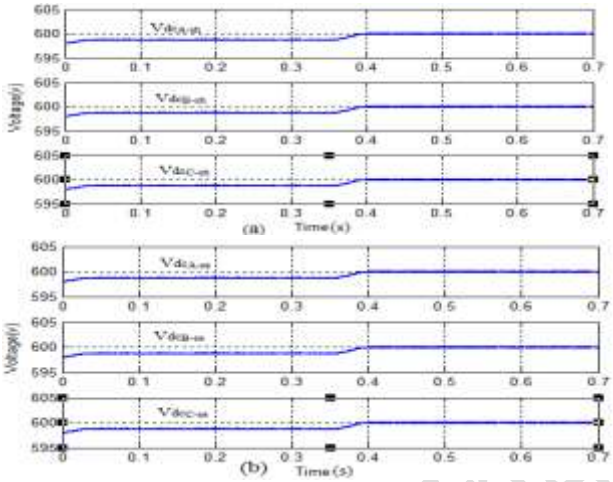

Fig. 13. (a) dc capacitor voltage of each phase of shunt CMI, (b) dc capacitor voltage of each phase of series CMI.

B. Line Impedance Compensation

The line impedance compensation is different from the phase shifting, where a voltage $\vec{V}_C$ is injected by the series CMI, which is in quadrature with the line current. Functionally it is analogous to series capacitive or inductive compensation by SSSC. Three operating conditions are shown in fig. 14. They are: (a) case B1: line impedance is equal to 0.5 p.u. (without compensation), (b) case B2: line impedance is equal to 1 p.u. (after compensation) and (c) case B3: line impedance is equal to infinity. In case B1 (same as case A3), phase difference between $\vec{V}_S$ and $\vec{V}_R$ is equal to 30°, as a result line current is 1 p.u. (amplitude 14 A).

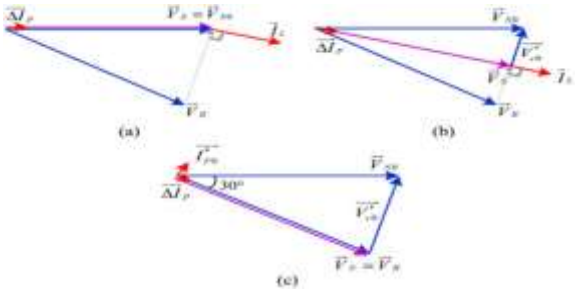

Fig. 14. Operating points (a) case B1: line impedance = 0.5 p.u., (b) case B2: line impedance = 1 p.u. and (c) case B3: line impedance after compensation = infinity.

The transformerless UPFC is also able to reduce the line impedance for higher line current. The results of UPFC when operating from case B1 to case B2 is shown in fig.15, where line impedance changed from 0.5 p.u. to 1 p.u. In this case the line current changed smoothly from 14A to 7A due to the increased line impedance.

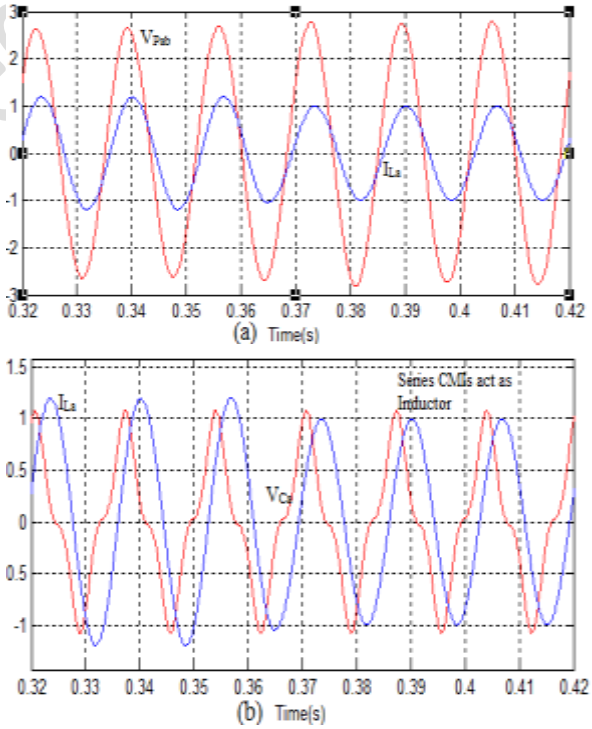

Fig. 15. Waveforms of UPFC when operating from case B1 to case B2 (a) line current I_{La} and shunt CMI line voltage $V_{P\,ab}$, (b) line current I_{La} and series CMI phase voltage $V_{C\,a}$.

It can be seen from Fig. 15(b) line current I_{La} is lagging V_{Ca} by 90° that means the series CMIs act

as inductors. It is the reason behind increasing line impedance from 0.5 to 1 p.u after compensation.

C. Independent P/Q Control

The transformerless UPFC has the ability to control the magnitude and phase angle of the injected voltage so as to maintain or vary the real and reactive power flow over the line according to the load demand and operating conditions of the system, i.e., independent P/Q control.

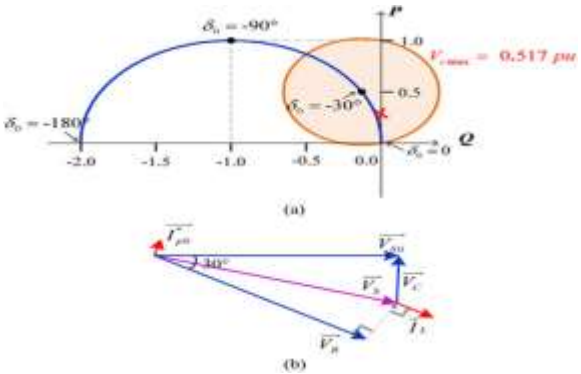

Fig. 16. Independent P/Q control (a) control region of the manageable real and reactive power at series CMI voltage = 0.517 p.u. and δ0= − 30◦, (b) case C1: P = 0.25, Q = 0.

In the fig. 16(a), the blue curve represents the transmittable real power P and reactive power Q vs phase angle δ0 of receiving end voltage and the circle represents the control region of the manageable real and reactive power at voltage of series CMI is equal to 0.517 p.u. and phase angle of receiving end voltage is equal to −30◦.

Usually, at any given δ0, the transmittable real power P as well as reactive power Q within the circle can be controlled by the UPFC. Several operating points of independent P/Q control have been tested [14]. Here, we have taken one of the test cases, case C1: P = 0.25, Q = 0, shown in Fig. 16(b).

In this case, because of zero reactive power, line current I_L is in phase with receiving-end voltage $\overrightarrow{V_R}$ and the amplitude of the line current is 7.5A and the results are shown in below fig. 17.

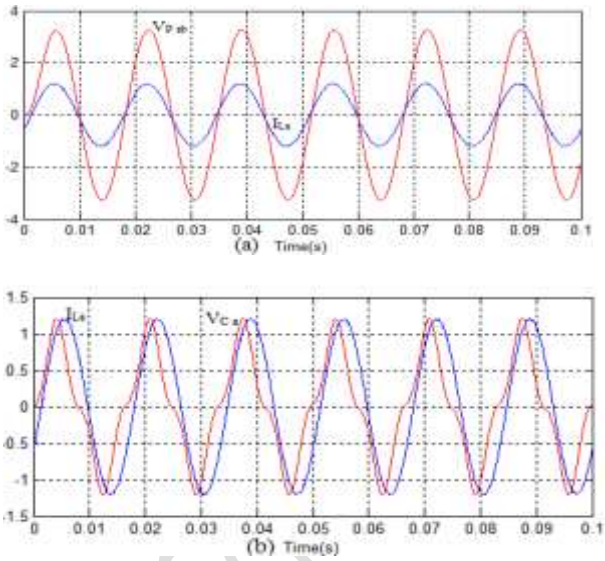

Fig. 17. Waveforms of UPFC at C1: P = 0.25, Q = 0: (a) shunt CMI line current I_{La} and line voltage $V_{P\ ab}$ and (b) line current I_{La} and series CMI phase voltage V_{Ca}.

D. Performance analysis of FL based UPFC for THD

This case is simulated to test the performance of proposed FL based UPFC for total harmonics distortion (THD) alleviation. THD of the different parameters of transmission line at different cases is shown in Table IV.

Table IV

THD (%) values for different parameters at different cases

	PI [15]				FUZZY			
	V_{Pab}	I_{La}	I_{Pa}	V_{Ca}	V_{Pab}	I_{La}	I_{Pa}	V_{Ca}
Case A1 to A2	3.61%	0.79%	42.12%	-	0.70%	0.29%	31.79%	-
Case A2 to A3	5.33%	0.69%	-	-	0.95%	0.69%	-	-
Case B1 to B2	5.34%	0.67%	-	38.62%	0.89%	0.26%	-	27.9%
Case C1 to C2	38.82%	0.80%	-	6.19%	25.44%	0.79%	-	0.09%

Where, V_{Pab}, I_{La}, I_{Pa} and V_{Ca} are the series CMI phase voltage, line current over the transmission line, shunt CMI phase current and series CMI phase voltage respectively. On contrast, the THD of different parameters of the line are reduced to some extant for FL based UPFC. Thus, the proposed FL based transformerless UPFC has effectively minimized the THD compared to PI based UPFC [15]. THD values of one of the cases (C1 to C2) for both the controllers are shown in Figs. 18 & 19.

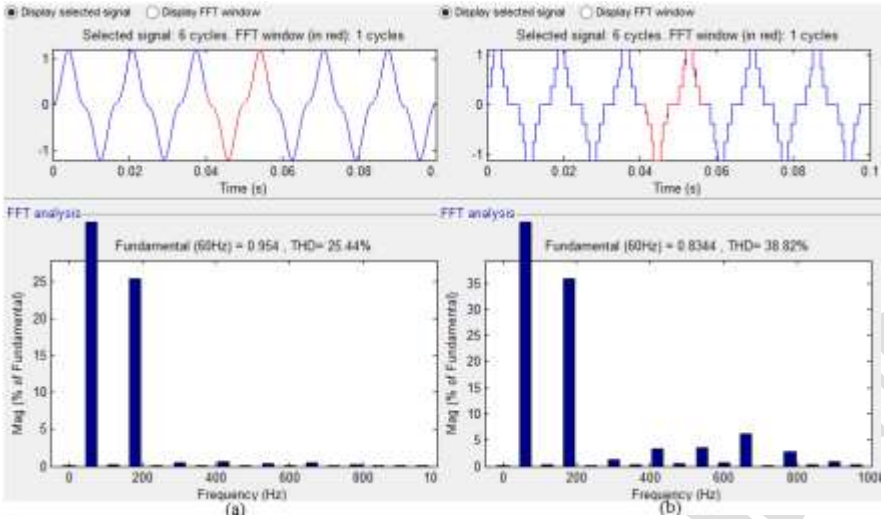

Fig. 18. (a) THD (%) value of V_{Pab} for fuzzy controller, (b) THD (%) value of V_{Pab} for PI controller.

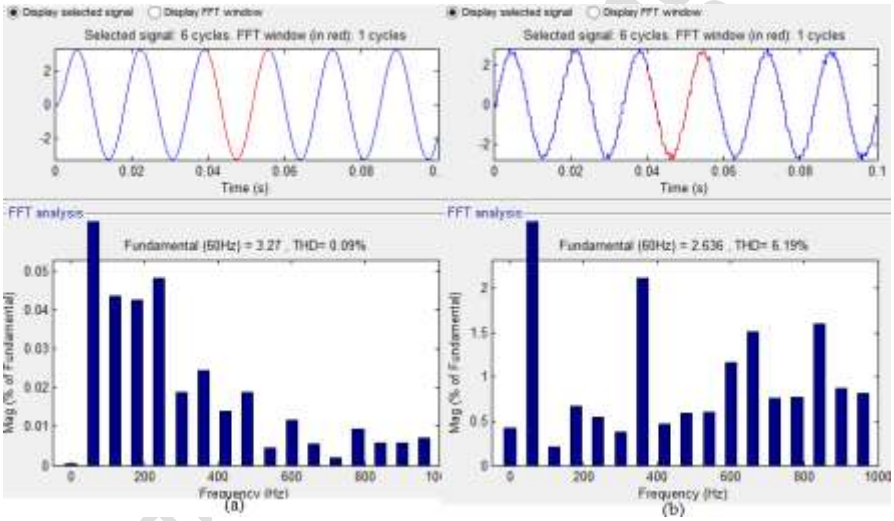

Fig. 19. (a) THD (%) value of V_{Ca} for fuzzy controller, (b) THD (%) value of V_{Ca} for PI controller.

CONCLUSION

A fuzzy controller based transformerless UPFC is presented to mitigate THD (Total Harmonic Distortion) over the transmission line, which in turn improves the efficiency of the system. To show its effectiveness, the performance of proposed FL based transformerless UPFC has also been compared with PI based transformerless UPFC for all the mentioned parameters. The THD of the series CMI phase voltage (V_{Pab}) in case C1 to C2 is reduced to 25.44% from 38.82%, when fuzzy controller is used instead of PI. It also improves the dynamic response (<8 ms) of the system. The transformerless UPFC based on FLC with proposed modulation and control can be installed anywhere in the grid to improve the power transmission over the grids, lessen transmission congestion..

REFERENCES

[1] L.Gyugyi, C.D. Schauder, S. L.Williams, T. R. Rietman, D. R. Torgerson, and A. Edris, "The unified power flow controller: A new approach to power transmission control," *IEEE Trans. Power Del.*, vol. 10, no. 2, pp. 1085– 1097, Apr. 1995.

[2] N. G. Hingorani and L. Gyugyi, "Understanding Facts: Concept and Technology of Flexible AC Transmission Systems," *Piscataway, NJ, USA: IEEE Press, 2000.*

[3] K. Sano and M. Takasaki, "A transformerless D-STATCOM based on a multi voltage cascade converter requiring no DC sources," *IEEE Trans. Power Electron.*, vol. 27, no. 6, pp. 2783–2795, Jun. 2012.

[4] B. A. Renz, A. Keri, A. S Mehraban, C. Schauder, E. Stacey, L.Kovalsky, L.Gyugyi,and A.Edris,"AEP unified power flow controller performance," *IEEE Trans. Power Del.*, vol. 14, no. 4, pp. 1374–1381, Oct. 1999.

[5] J. Wang and F. Z. Peng, "Unified power flow controller using the cascade multilevel inverter," *IEEE Trans. Power Electron*, vol. 19, no. 4, pp. 1077–1084, Jul. 2004.

[6] F. Z. Peng and J. S. Lai, "Dynamic performance and control of a static var generator using cascade multilevel inverters," *IEEE Trans. Ind. Appl.*, vol. 33, no. 3, pp. 748–755, May/Jun. 1997.

[7] F. Z. Peng and J. Wang, "A universal STATCOM with delta-connected cascade multilevel inverter," *in Proc. Annu. IEEE Power Electron. Spec. Conf.*, 2004, pp. 3529–3533.

[8] B. Gultekin, C. O. Gercek, T. Atalik, M. Deniz, N. Bicer, M. Ermis, K. N. Kose, C. Ermis, E. Koc, I. Cadirci, A. Acik, Y. Akkaya, H. Toygar, and S.Bideci, "Design and implementation of a 154-kV 50-Mvar transmission STATCOM based on 21-level cascaded multilevel converter," *IEEE Trans. Ind. Appl.*, vol. 48, no. 3, pp. 1030–1045, May/Jun. 2012.

[9] H. Fujita, Y. Watanable, and H. Akagi, "Transient analysis of a unified power flow controller and its application to design of dc-link capacitor," *IEEE Trans. Power Electron.*, vol. 16, no. 5, pp. 735–740, Sep. 2001.

[10] J. Wang and D. Ahmadi, "A precise and practical harmonic elimination method for multilevel inverters," *IEEE Trans. Ind. Appl.*, vol. 46, no. 2, pp. 857–865, Mar./Apr. 2010.

[11] L. Liu, P. Zhu, Y. Kang, and J. Chen, "Power-flow control performance analysis of a unified power-flow controller in a novel control scheme," *IEEE Trans. Power Del.*, vol. 22, no. 3, pp. 1613–1619, Jul. 2007.

[12] S. Kouro, R. Bernal, H. Miranda, C. A. Silva, and J. Rodriguez, "High performance torque and flux control for multilevel inverter fed induction motors," *IEEE Trans.PowerElectron.*,vol.22,no.6,pp.2116–2123,Nov.2007

[13] H.Fujita, H. Akagi, and Y.Watanable, "Dynamic control and performance of a unified power flow controller for stabilizing an AC transmission system," *IEEE Trans. Power Electron.*, vol. 21, no. 4, pp. 1013–1020, Jul. 2006.

[14] S. Y. Kim, J. S. Yoon, B. H. Chang, and D. H. Baek, "The operation experience of KEPCO UPFC," *in Proc. 8th Int. Conf. Electr. Mach. Syst.*, 2005, pp. 2502–2505.

[15] Shuitao Yang, Yang Liu, Xiaorui Wang, Deepak Gunasekaran, Ujjwal Karki, and Fang Z. Peng, "Modulation and Control of Transformerless UPFC" *IEEE Trans. Power Electron.*, vol. 31, no. 4, February 2016.

[16] T Jagan Mohan Rao, P Anil Kumar, Ch. Krishna Rao "Voltage Source Inverter/Converter for the Improvement of Power Quality Using Fuzzy Logic Controller" *ISSN: 2248-9622*, Vol. 4, Issue 5(Version 1), May 2014, pp.46.